Electron Delocalization and Electrochemical Potential Distribution Phenomena in Faradaic Electrode Materials for Understanding Electrochemical Behavior

Yachao Zhu, Siraprapha Deebansok, Jie Deng, Xuanze Wang, Thierry Brousse, Frédéric Favier, Olivier Fontaine

Electron delocalization and electrochemical potential distribution phenomena in Faradaic Electrode Materials for understanding electrochemical behavior

Yachao Zhu,[1#] Siraprapha Deebansok,[2#] Jie Deng,[3] Xuanze Wang,[2] Thierry Brousse,[4,5] Frederic Favier,[1,5] Olivier Fontaine [2*]

[1] ICGM, Univ Montpellier, CNRS, Montpellier, France.

[2] Molecular Electrochemistry for Energy Laboratory, School of Energy Science and Engineering, Vidyasirimedhi Institute of Science and Technology (VISTEC), Rayong, 21210, Thailand.

[3] Institute for Advanced Study, Chengdu University, Chengdu 610106, China

[4] Nantes Université, CNRS, Institut des Matériaux de Nantes Jean Rouxel, IMN, , 2 rue de la Houssinière BP32229, 44322 Nantes cedex 3, France

[5] Réseau sur le Stockage Electrochimique de l'Energie (RS2E), CNRS FR 3459, 33 rue Saint Leu, 80039 Amiens Cedex, France

[#] These authors contributed equally

* Corresponding author. Email: Olivier Fontaine: olivier.fontaine@vistec.ac.th

Abstract

Electrochemical energy storage devices are built upon the foundations of batteries and supercapacitors. In the past decade, new types of electrode materials, such as pseudocapacitor-like species, have been intensively developed to obtain superior performance in terms of energy density and powder. Pseudocapacitive materials store charge through Faradaic redox processes, while their electrochemical signature remains mystically similar to that of electrochemical double-layer capacitors, even though it is caused by redox processes. To address this controversy, we introduce an all-inclusive analytical model for evaluating the voltammograms of electrode materials. In view of this, the present article focuses on understanding the origin of the pseudocapacitive phenomena in the electrochemical signal (such as cyclic voltammetry, CV). Based on the self-exchange electron transfer mechanism and tunneling effect within the atomic structure of solid electrode materials, pseudocapacitive materials possess a high degree of electron delocalization possibility related to the number of redox centers. This process initiates the electrochemical potential distribution among the neighboring redox sites, which is consequently observed in electrochemical signal as the plateau feature in CV like in EDLC. We proposed for the first time the determination of capacitive tendency of various faradaic electrode materials, which turned out to be relative to the number of redox center (n) and total charge (z) as presented in this work as a functional type of electrode material classification plot. Here, we proposed the theoretical link of electron hopping, likely occurring when the number of redox centers are large. The developed all-inclusive model is versatile to predict rate/potential regimes for the maximum faradaic storage, and then well differentiates the pseudocapacitor- materials from battery- materials.

Introduction

The ever-growing global demand for energy underwent a sharp and sudden increase, leading to the expansion of energy storage technologies. Many of these storage technologies, most notably electrochemical energy storage, rely on redox processes[1]. The chemical composition of electrodes has been the topic of many studies to improve the performance of electrode materials in terms of energy and power densities [2, 3]. Within this multiplicity of compositions, nanostructures and properties, electrode materials are classified into two categories: non-Faradaic and Faradaic electrode materials. A non-Faradaic reaction points to one in which there is an absence of electron exchange across the electrode-electrolyte interface. In this case, charge storage occurs as a consequence of charging the electrochemical double layer at the electrode-solution interface. When Faradaic processes are engaged, however, electrons are transferred across the current collector to or from redox centers contained inside the electrode. Redox centers are buried in a solid phase, and the charging process thus involves the motion of counterions. The difference between these electrode materials is electrochemically detectable and is analyzed according to their physicochemical traits. Numerous characteristics are determined using a variety of methods, including electrochemical impedance spectroscopy and cyclic voltammetry (CV) [4, 5]. The CV technique has the advantage of varying the cell voltage (or potential, in a 3-electrode system) and observing the impact of these fluctuations on the cell dynamics (i.e., electron and ion transfer), while modulating the scan rate, *i.e.*, the time scale of the material studied.[6] While non-Faradaic electrode materials produce a box-shaped signal during CV measurements, Faradaic electrode materials present current peaks, indicating the potential value of their redox center.[7] However, Faradaic electrode materials are only seldom amenable to analysis through a perfect Gaussian peak signal, as idealized by the notion of immobilized redox centers (**Fig. S2a**). Similarly, a thorough examination of the

i=f(E) curves reveals that Gaussian peaks are not perfectly symmetrical (see **Fig. S2b** for the ideal electrochemical response).

Surprisingly, there are no contemporary theories or formalist frameworks that make clear the story of faradaic materials well. To compound the issue, many more questions arise when addressing pseudocapacitive materials, which are characterized as Faradaic electrode materials that exhibit a box-shaped signature during a current-potential measurement (CV) [8]. Two unsolved questions today are: firstly, how might it be possible to sign a Faradic phenomenon with a curve comparable to that of an electric double-layer capacitor (EDLC) material when the established signature must be Gaussian; secondly, which similarities and differences are present when comparing a Gaussian ideal material to a material with pseudocapacitive properties? The pseudocapacitor's box-shaped CV has been observed in a wide variety of transition metal oxides [9], conducting polymers [10], and other semiconducting redox materials. The mechanisms by which Faradaic reactions may exhibit quasi-rectangular capacitive electrochemical behavior remain unknown, and no cohesive model explaining the peculiarities of Faradaic electrode materials exists in the literature. Numerous studies, however, serve to demonstrate this pseudocapacitive behavior (**Fig. S1**) [2, 4, 11-44]. This thus leads one to consider the possible reasons for a redox reaction, which is essentially a Faradaic occurrence, deviating so far from the ideal peak response (as illustrated in **Figure 1**).

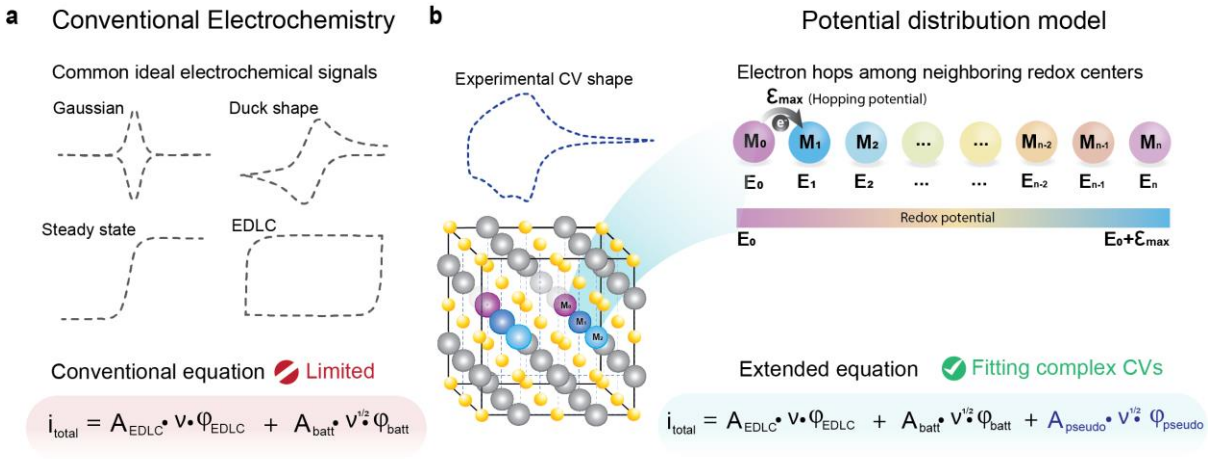

Fig. 1 | (a) Conventional electrochemistry signals in ideal CVs with the conventional equation are limited to describe only simple CVs. (b) Potential distribution model within the electrode material structure based on electron transfer between redox centers (M_0, M_1, …, M_n) with the redox potentials respectively to each redox site. And our new extended equation for the total current leads to the first-time complex CV fitting.

Fig. S3a illustrates the many and varied Faradaic electrode materials (*i.e.*, those concerned with electron transfer), including both those used in pseudocapacitors as well as those used in batteries. Regardless of which technical device is concerned, the electrode component, including its active material, stays constant. The active material stores charges through redox reactions involving the crystalline structure's redox center (as illustrated in **Figure 1**). As a result, this active material may be regarded as a matrix, with redox centers being connected by covalent bridges (**Fig. S3b**, *e.g.*, oxygens) that lead these redox centers to interact. Naturally, the true nature of materials remains multifaceted, including hierarchical porosity, multicrystalline structures, the presence of binders, conductive additives, and the percolation of highly conductive carbons near oxide particles.

In order to comprehend and rationalize the wide range of electrochemical reactions observed in Faradaic electrode materials (including pseudocapacitive materials), a three-step strategy is provided herein. The first step involves categorizing the relevant materials according to their n (number of redox centers per nm^3) and Z (electron included in crystalline structure) values. These parameters bring the effect of the n and Z values on the electrochemical signature to light. In the second step, the influence of n and Z is then rationalized using a certain microscopic approach centered on electron transfer (*i.e.*, the transition-state model). The third and final step, enabled by the first two in terms of creating a collection of parameters, makes use of these to simulate and compare theoretical and experimental electrochemical signal responses.

Results and discussion

As stated before, there is no available model that combines the behavior of a battery with that of a pseudocapacitor currently. To complicate matters, these concepts are often separated into two distinct categories. This means that researchers find themselves without a coherent, universal method for analyzing and decoding electrochemical behavior (*i.e.*, the shape of the cyclic voltammogram). A unified technique could be considered a significant step towards the future development of innovative, high-power batteries. We thus propose an integrated model, demonstrating that pseudocapacitive contributions indeed also exist in battery materials (Li-ion, Na-ion, Mg-ion). CVs of batteries demonstrating their cell dynamics (electron and ion transport) are also shown to deviate significantly from the ideal signals published in the 1980s.

The number of redox centers per nm^3 and the Z value as simple markers for distinguishing between pseudocapacitive and battery materials

The primary goal is to be able to compare Faradaic electrode materials using three simple markers: (i) n, the number of redox centers per nm^3 calculated as described in the Supporting Information (Section 5), (ii) Z, the number of electrons included in the crystalline structure, and (iii) *capacitive tendency*, the ratio of peak current to plateau current is named pseudocapacitive percentage. The number of redox centers per cubic nanometer and the number of electrons per crystalline structure were determined for a series of lithium-ion batteries and pseudocapacitive materials. We compiled a list of fifty materials that are the most often used in electrochemical energy storage devices. Furthermore, we established a new parameter, *the capacitive tendency*. Capacitive tendency is the parameter to describe the electrochemical behavior of materials. This predictive model was published by some of us.[115], using deep learning to classify electrochemical signals. The specific research involves using image classification to distinguish different curve shapes (rectangular shape and peak shape) that act on electrochemical signals, such as cyclic voltammetry, to connect electrochemical information (pseudocapacitor and batterie). When the capacitive tendency is close to 100%, the curve is more rectangular, and the material is more like a supercapacitor. When the capacitive tendency is close to 0%, the curve is more like a peak shape and the material is more like a battery. The capacitive tendency analyzes the shape of the voltammogram.

The capacitive tendency and capacitive contribution are not the same concept. *Bruce Dunn et al.*[116] proposed a model in 2007 that is proportional to current and scan rate, and used this model to describe the capacitive contribution and diffusion contribution in materials. The capacitive contribution is different from capacitive tendency proposed by some of us, because the capacitive tendency is a metric to describe the shape of the material's signal curve and classify the material, rather than to calculate the proportion of capacitive contribution inside the material or provide the percentage of EDLC, pseudocapacitor or battery.

Alternatively, there is an another simple way to calculate and express rectangular shape, which is called capacitive percentage, or simply *%capa* (see ESI section 5 and Fig. S5). Equation 1 defines this pseudocapacitive percentage, but this result is just an approximate result. This one can only explain the general trend, and capacitive tendency is the result more accurate.

$$\%_{capa} = 100 - \frac{i_{max} - i_{min}}{i_{max}} \cdot 100 \qquad \text{Eq. 1}$$

Where i_{max} is the maximum current and i_{min} is the relative minimum current taken after the faradaic contribution. **Figure 2** shows a heatmap of capacitive tendency of all materials researched in the work.

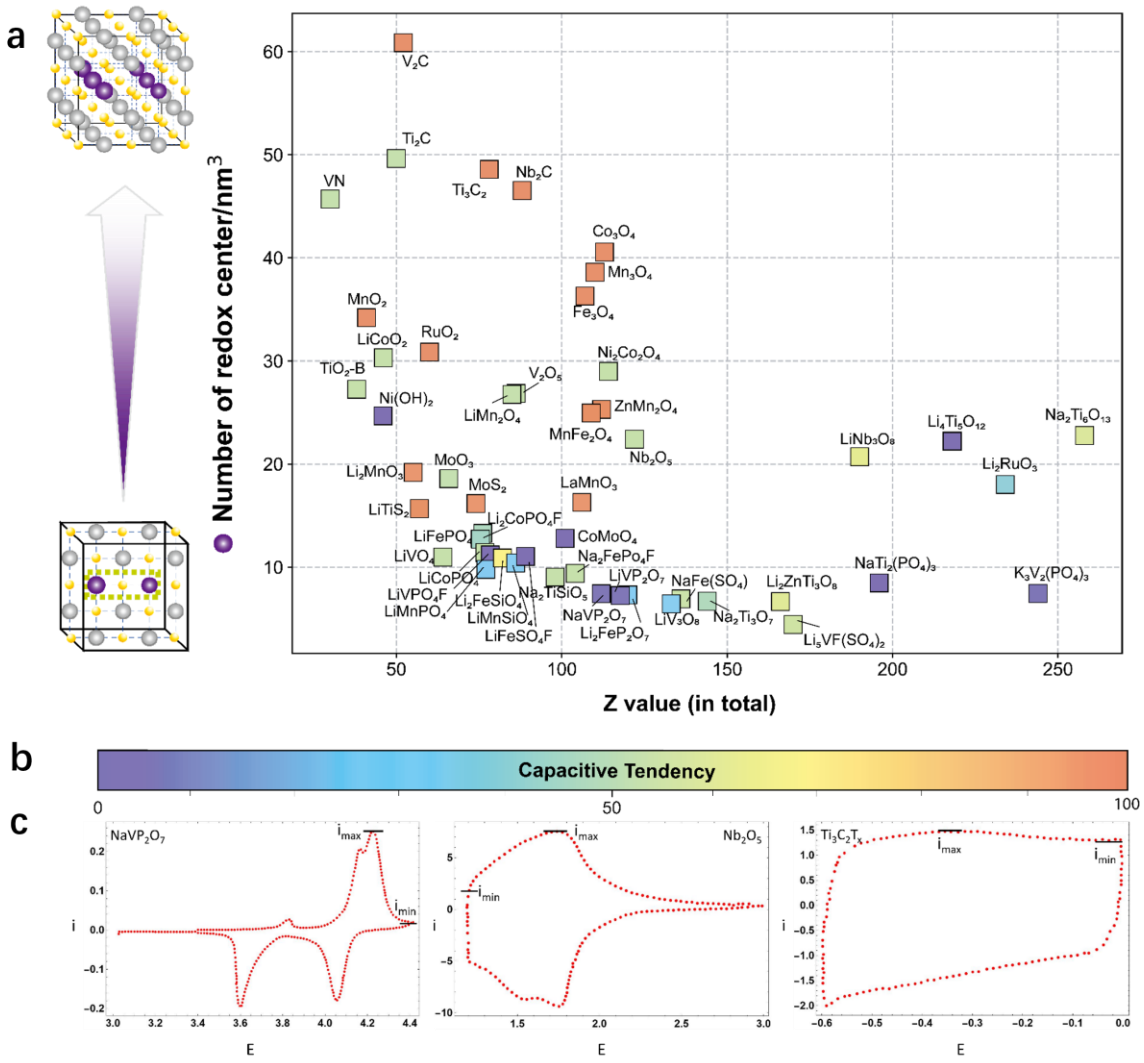

158

159 **Figure 2. State-of-the-Art in Faradaic electrode materials for batteries and**
160 **pseudocapacitors**. (a) represents a list of materials classified according to capacitive tendency
161 (ascribed to the color bar). The Y-axis represents the number of redox centers per nm^3 and the
162 X-axis represents the total number of electrons in the crystal structure. (b) the qualitative color
163 bar representing capacitive tendency. (c) represent typical voltammograms of the
164 corresponding electrode material.

165 This computation makes it possible to account for the nuances inherent in the
166 voltammogram shapes as measured in the CV experiments. The $\%capa$ is a useful indicator
167 when it comes to anticipating the degree of charge delocalization. On the one hand, if the local
168 minimum current is close to the maximum current, then the current is identical and the behavior

displayed is rectangular (noting that the global resistance of the device is not taken into account in the calculation). This rectangular voltammogram represents the signature of so-called supercapacitive substances, be they EDLCs or pseudocapacitors. On the other hand, if the difference is significant, *i.e.*, the redox peak is highly prominent, then the behavior displayed is battery-like. Indeed, in order to accurately depict the electrochemical behavior of the real-world voltammograms, calculating the $\%pseudo$ thus allows for a simple categorization of the voltammogram shape, regardless of the material composition or lack thereof. The *capacitive tendency* is a graphical descriptor of a curve *i=f(E)* that is independent of the usual material classification (battery, EDLC, pseudocapacitor).

The result of combining the redox center number per nm^3 with the electron number Z of the crystalline structure is shown in Fig. 2. The cell count is based on the volume of each cell (see the CIF file, in ESI), and the cell unit's Z' value indicates the number of material crystalline units repeated in one cell volume. In addition, capacitive tendency is used for over forty materials involved in the manuscript and compared it with the %pseudo results calculated from Equation 1, the complete result table is Table S4 in ESI.

In **Fig. 2, S7-S8**, a scatter plot with a gradient of different colors denoting the *capacitive tendency* is used to position the 50 different materials [5, 45-91]. Each of these materials is accompanied by voltammograms which were extracted from scientific publications. They were selected due to the fact that they are the most frequently applied materials in batteries and pseudocapacitors. For decades, these materials have been in constant evolution with the synthesis of new materials, the design of new structures, adjustments to their inner nature, and modifications to their morphology, all of which were geared towards maximizing the capacitance/capacity to build advanced energy storage devices. As far as pseudocapacitive materials are concerned, RuO_2 stands out as one that underwent years of trials before finally shedding light on the mechanism of redox reactions in aqueous acidic electrolytes. This had to

do with the valence change from Ru^{4+} to Ru^{3+}/Ru^{2+}, associated with proton insertion [92-93]. Another prominent one is MnO_2 , which possesses a smooth ionic diffusion but displays limited electronic conductivity [9]. These two laid the groundwork for further research involving metal oxide-based Faradaic electrode materials, such as TiO_2, Nb_2O_5, Co_3O_4, Mn_3O_4, Fe_3O_4, etc. In the case of Co_3O_4, it was found that morphological changes and size could lead to distinctive electrochemical behavior, since when nanosized it triggers a high-rate redox reaction.[105] Aside from metal oxides, carbides and nitrides (*e.g.*, vanadium nitride) also become the subject of research relating to redox reactions in pseudocapacitive materials. Among them, 2D MXenes, such as Ti_3C_2, Ti_2C, V_2C, prevail due to their intriguing electronic conductivity and high-rate capability [106, 107]. Numerous battery materials have been studied for use as anodes and cathodes in various battery cells. Current cathode materials that have already been commercialized include the well-known $LiCoO_2$ and $LiFePO_4$ (ref 94). On the anode side, the most notable are $LiTi_4O_5$ and TiO_2 (ref 95). It has been ascertained that battery materials exert redox reactions following phase changes after intercalating [108-111]. The materials selected for this study all serve to contribute to an overall picture of Faradaic electrode materials.

We observe an unmistakable trend whereby pseudocapacitive materials display a redox center density of between 20 and 60 per nm^3 and a Z value of between 0 and 120. In other words, a pseudocapacitive material has a large number of redox centers with a low number of electrons inside its crystalline structure. For battery materials, the number of redox centers are never greater than 30 per nm^3, while Z values can reach up to 140.

More specifically, MnO_2 and RuO_2 both show a *capacitive tendency* of close to 100% with a large number of redox centers per nm^3 and low Z values. Mn-based materials can be battery-type ones such as Li_2MnO_3 (ref 85), Li_2MnSiO_4 (ref 91) and $LiMnPO_4$ (ref 59) or pseudocapacitor-type ones such as MnO_2 (ref 13). The same goes for Ti, with battery-type ones such as $LiTiS_2$ (ref 80), Na_2TiSiO_5 (ref 54), $NaTi_2(PO_4)_3$ (ref 78), $Li_4Ti_5O_{12}$ (ref 66) and $Na_2Ti_6O_{13}$ (ref 81),

and pseudocapacitor-type ones such as Ti_2C [ref 29] and Ti_3C_2 [ref 11]. Some materials are not a good fit for this simple classification, such as MoS_2 [ref 51] and MoO_3 that show around 17 redox centers per nm^3 and a Z value of around 70, all the while displaying pseudocapacitive behavior. Co_3O_4, Mn_3O_4 and Fe_3O_4 exhibit large densities of redox centers together with high Z values, with *capacitive tendency* values of around 50%. 2D MXene materials, including Ti_3C_2 and V_2C, are pseudocapacitive materials with high redox center densities and low Z values. It should be noted that the choice of electrolyte probably has an impact on the *capacitive tendency* value. For example, for $Ti_3C_2T_x$-MXene [ref 29], the *capacitive tendency* value decreases from 80 to 50% (in KOH and H_2SO_4, respectively). V_2C-MXene [ref 72] shows similar results. Concerning MnO_2 in an aqueous medium, the electrochemical reversibility can be highly impacted depending on the pH. This can be explained by a confinement phenomenon, where a transition occurs from double-layer to Faradaic charge storage.[114] The electrochemical interface actually involves porous or layered cases instead of an ideal planar model. With increasing interface complexity, charge transfer improves between an electrolyte ion and the host regarding the extent of ion desolvation and confinement. When K^+ intercalates in birnessite metal oxide, the K^+ is still hydrated without desolvation between interlayers, which offers a weak ion-host interaction and reduced charge transfer.

We have demonstrated that identifying the density of redox centers, *n*, and the corresponding *Z* values is enough to accurately predict the material type and the global shape of the cyclic voltammogram and vice versa. For the greater part of the researchers working in the field of electrochemical energy storage materials, determining the *n* and *Z* parameters will thus be quite straightforward. However, it is worth noting that the type of salt and nature of the solvent used in the electrolyte may sometimes affect the electrochemical behavior, and therefore the shape of the voltammogram.

To summarize, the *capacitive tendency* , and consequently the shape of the voltammogram, is chiefly governed by: (1) the number of redox centers per nm^3, and (2) the Z value of the crystalline structure, bearing in mind that (3) the nature of the electrolyte may have a certain effect on the result. It is then necessary to correlate these pieces of information within a model that explains why these three parameters affect the voltammogram signal. To this end, it is necessary to understand the impact that the proximity of the density of redox centers, n, has on the electron moving through the Faradaic electrode material.

Electron movement as a cause of redox potential distribution

The initial Faradaic oxidative reactions that generate charges in the material are likely connected to ionic mobility, independently of the pseudocapacitive or battery-like behavior of the considered material. Therefore, the fundamental process of electron injection into a redox center remains a redox reaction, which is a Faradaic phenomenon. However, the spatial organization and density of the redox centers in battery and pseudocapacitive materials can produce quite a different outcome. The density of redox centers has a direct impact on the probability of an electron jumping from one redox center to another. Pseudocapacitive materials exhibit a large number of redox centers per nm^3, with a total exceeding 30. Following a charge injection (or extraction), the charge distribution then creates a distribution of redox potentials (as demonstrated in the following section). To explore this effect, we will first demonstrate that the probability of transferring an electron between two redox centers is greater when n is large and Z is small. In a subsequent step, we will show that an electron exchanged between two redox centers has an effect on the potential of neighboring centers.

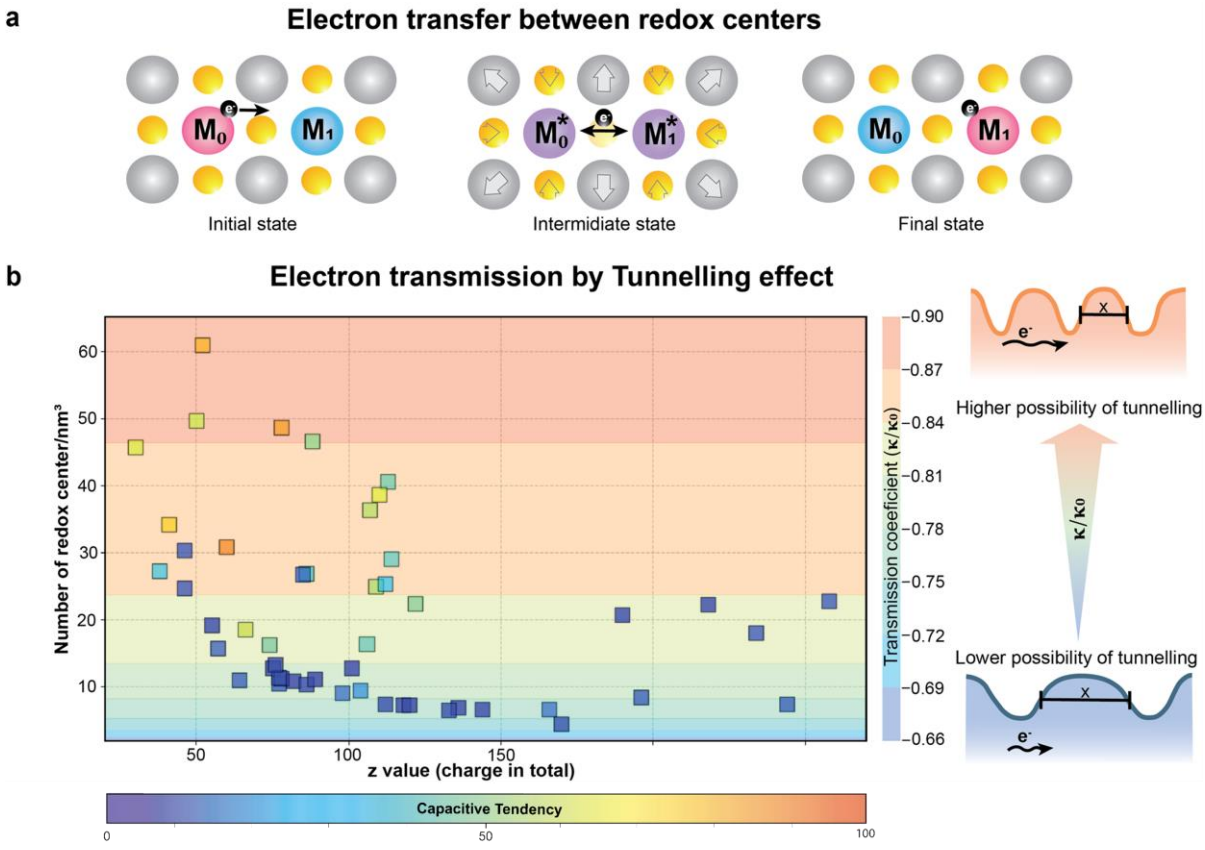

Figure 3. Electron transfer between 2 redox centers. (a) represent the atomic changes associated with electron transfer for a solid structure. (b) represents the electron transfer probability as a function of the number of redox centers (Y-axis). The background color is respected to the transmission coefficient of electron transfer according to tunnelling effect.

To understand the possibility of an electron exchange between two redox centers, the probability of an electron hopping from one redox center to another may be expressed as the product of three separate probabilities. The first probability is equivalent to the chances of the electron encountering a neighboring redox center (noting that a defect in the crystalline structure will reduce this probability). The second probability is that a phonon (the vibration of a crystal lattice) causes the local distortion necessary for the temporary equalization of donor

and acceptor levels (**Fig 3a**). The third probability is that tunneling occurs (**Fig.3b**), which is exponentially dependent upon the distance between the two considered redox centers.

According to this formalism, the greater the density of redox centers, the greater the probability of the electron being delocalized. This is consistent with the fact that a pseudocapacitive material has a large number of redox centers per nm^3, so the probability of charge delocalization is non-zero. It is worth noting that in the preliminary reports about the redox behavior of RuO_2, Trasatti *et al.*[96] emphasized this fact from the very start, stating, with respect to the metal cores, that the "*Me-Me* distance and the radius of the cation in these oxides are such that overlap of the inner d orbitals is possible, and the d electrons in the d bands are responsible for the metallic conduction", referring to Marcus studies on electron transfer to substantiate this remark [97].

One particular “chemical” description of the proximity of the redox center may be investigated as a reaction comprising electron hopping. There are two alternatives when an electron is injected into a redox center: (1) The injected electron is restricted to the vicinity of the redox center (*i.e.*, it is localized), or (2) the electron jumps to the nearest neighbor. After that, the charge is partially delocalized. This viewpoint is comparable to that of adiabatic vs. diabatic electron transfer [98].

Now, the electron transfers or hops from one redox center to the neighboring one in the electrode material structure. The redox reaction can be transcribed, along with the associated ionic transfer (where *A* is the anion) with equilibrium constant with the equilibrium ($K_{hopping}$) as follows:

$$A \cdot M^{(a+1)+} + M^{(a-1)+} \underset{k_{-1}}{\overset{k_1}{\rightleftarrows}} \underbrace{M^{(a)+} + M^{(a)+}}_{A} \qquad \text{Eq. 2}$$

where a is the reaction activity of a certain state.

If $k_1 \gg k_{-1}$ ($K_{hopping} \gg 1$) then the probability of an electron exchange between 2 redox centers is high. And inversely, if $k_1 \ll k_{-1}$ ($K_{hopping} \ll 1$), then the probability of an electron exchange is low. According to this equation, the way in which the redox charge is shared is based on an equilibrium constant, $K_{hopping}$. This equilibrium constant can then be expressed as the difference in redox potential required in order to oxidize both redox sites. E_0 is the potential to oxidize the first one, the so-called standard redox center, and E_1 is the redox potential of the closest neighbor.

E_n corresponds to the redox potential of the umpteenth neighbor, then the umpteenth neighbour, $K_{hopping,n}$ is:

$$K_{hopping,n} = exp\left[\frac{F\cdot(E_n - E_0)}{R\cdot T}\right] \quad \text{Eq. 3.}$$

Where F is the Faraday constant (96485 in $C \cdot mol^{-1}$), R is the gas constant (8.3145 $J \cdot mol^{-1} \cdot K^{-1}$), and T is temperature (293.15 K).

The equation **Eq. 3** highlights two critical points: (i) Firstly, when two redox centers easily exchange electrons ($K_{hopping,1} \gg 1$), then the difference in potential between the two redox centers is quite large ($E_n - E_0$>>0). In other words, injecting a charge into one of the redox centers has an effect on the amount of work required to inject a charge into the redox center closest to it. (ii) Secondly, the further away a neighbor is from the standard redox center, the less likely it is for them to share an electron. The potential distributes from the first redox center (M_0) to the nearest (M_1) and other neighboring redox centers (M_n) with hopping potential (ε).

n is the total number of potential hopping in the system, which corresponds to the number of neighbors nearest to the area where tunneling is likely to occur. ε_{max} and ε_{min} are the maximum and minimum potential difference between two redox centers as demonstrated in Figure 4.

The neighboring redox centers (M_i, when $i = 1, 2, 3, \dots, n$ and i is the neighbor according to its position with respect to the standard redox center), the potential distributed is in descending order:

$$E_1 > E_2 \gg E_n > E_{n+1} \approx E_0$$

Then, $K_{hopping,1} > K_{hopping,2} > K_{hopping,3} \gg K_{hopping,n}$

Firstly, among n number of redox center, started from M_0.

$$M_0, M_1, \dots, M_{n-4}, M_{n-3}, M_{n-2}, M_{n-1}, M_n$$

At the farthest redox center (M_n), the lowest energy needed for the electron to jump, ε_{min}. By recurrence sequence, the hopping potential from the farthest to the nearest neighboring redox site is in ascending order:

$$n\varepsilon_{min}, \dots, 5\varepsilon_{min}, 4\varepsilon_{min}, 3\varepsilon_{min}, 2\varepsilon_{min}, \varepsilon_{min} \quad .$$

So, $$E_{n-i} = E_0 + (i+1)\varepsilon_{min} \qquad \text{Eq. 4}$$

When $i = 1,2,3, \dots, n$.

In this model of the redox potential distribution, there are three notable variables: ε_{max}, ε_{min} and n. So, ε_{max} is the work difference between the two nearest redox centers ($E_1 - E_0$). When a charge is injected into the standard redox center, its nearest neighbour has the most impacted electron affinity, so its redox potential is increased by a maximum jump (ε_{max}). Whereas the minimum potential jump corresponds to the furthest redox center influenced by the charge, noted by ε_{min}. Then n represents the number of neighbors influenced by the charge injection. Note that **Eq. 3** and **Eq. 4** then become, for the general form:

$$K_{ET,i} = exp\left[\frac{F \cdot \varepsilon_{max}}{i \cdot R \cdot T}\right] \qquad \text{Eq. 5,}$$

and, for the nearest neighbor ($i = 1$):

$$K_{ET,1} = exp\left[\frac{F \cdot \varepsilon_{max}}{R \cdot T}\right] \quad \text{Eq. 6,}$$

and, for the most distant neighbor ($i = n$):

$$K_{ET,n} = exp\left[\frac{F \cdot \varepsilon_{min}}{R \cdot T}\right] \quad \text{Eq. 7.}$$

Fig. S3 illustrates the matrix model, including the redox potential distribution, using **Eq. 4**. When redox centers are tightly packed together, the electron affinity decreases (*i.e.*, it is more difficult to inject the electron into the nearest neighbor). This model involves a large redox potential distribution within the material.

A Faradaic electrode material is thus represented by the matrix, for which the continuous phase represents the overall charge in the crystalline structure and where the color of the redox centers is the distribution of redox potentials. Therefore, the proximity of the redox centers – high-density *n* - results in a broad redox potential distribution, as illustrated by the matrix model.

The rate constant, k_1, which is the kinetic constant of the electron transfer, is expressed by considering two rate-limiting steps. The first step is to consider that the electron transfer is sequential to the ion transfer. Therefore, k_1 will either be the electron transfer or the transfer of the counter-ion to be split. However, an alternative to this could be that the electron transfer is concomitant with the ion transfer, so that the rate constant k_1 will reflect a new mathematical expression. Recently, Bazant *et al.* incorporated ion transfer effects into the kinetic theory of electron transfer[99]. The nature of the counterion can be varied: Such as Li^+, $Na^{+,}$ Mg^{2+}, Zn^{2+} etc.

Three phenomena influence the charge storage process in electrochemical energy storage materials: (1) the tunneling effect, (2) the chemical environment of the redox center, and (3) the effect of the counterion from the electrolyte. By analogy with the electron transfer in solution, therefore, a link on charge processes exist. The crystalline structure, the counterions and the distance between the redox centers all influence the ease with which charges can be

delocalized. The effect of the counterion also deserves careful consideration, since the kinetics of electron exchange will be influenced by its probability of being shared or not, resulting in charge delocalization. Significantly, the charge delocalization induced by these three phenomena results in a redox potential distribution within the Faradaic electrode materials. This framework thus allows one to pinpoint the fundamental differences between a wide range of Faradaic electrode materials. Unexpectedly, however, battery materials display a partial charge distribution, implying that their charging mechanism must include a pseudocapacitive contribution. This last point is crucial, as these two types of materials are frequently pitted against each other in the scientific literature. Nonetheless, we demonstrate herein, for the first time, that by using our inclusive model one sees a strong connection between these two types of materials and can observe the source of this distinction. This is achieved by associating the redox potential distribution model with an experimentally exploitable electrochemical signal.

Using the quantification of redox potential distribution to determine the electrochemical behavior of Faradaic electrode materials

Based on the probabilistic description of electron exchange through many redox centers, it is then necessary to create a model that incorporates the redox potential distributions of the electrochemical signals.

In this case, the signal would be the sum of the individual signals from *n* populations of redox centers, *n* being the variable developed in the previous section, *i.e.*, the number of neighbors impacted by the redox reaction of the so-called standard redox center. In a similar way to the EDLC current and the battery current, the current resulting from a pseudocapacitive contribution is expressed as:

$$\varphi_{pseudo} = \sum_{i=0}^{i=n=\frac{E^{f}_{pseudo}-E^{i}_{pseudo}}{\varepsilon}} \varphi^{i}_{pseudo} \qquad \text{Eq. 8.}$$

The contribution of the neighbor *i* would then be similar to the mathematical expression of the pure battery current as follows:

$$\varphi_{pseudo}^{i} = \frac{R\cdot T}{2\cdot F\cdot G}\cdot e^{\frac{F}{R\cdot T}\left(E_{apply}-\left(E_{pseudo}^{i}+n\varepsilon\right)\right)}\left(\frac{e^{\frac{F\cdot G}{R\cdot T}}}{1+e^{\frac{F\cdot G_{pseudo}}{R\cdot T}}\cdot e^{\frac{F}{R\cdot T}\left(E_{apply}-\left(E_{pseudo}^{i}+n\varepsilon\right)\right)}}-\frac{e^{\frac{-F\cdot G}{R\cdot T}}}{1+e^{\frac{-F\cdot G}{R\cdot T}}\cdot e^{\frac{F}{R\cdot T}\left(E_{apply}-\left(E_{pseudo}^{i}+n\varepsilon\right)\right)}}\right) \quad \text{Eq.9,}$$

where n is the number of potential hopping between redox centers (per nm^3), ε is the hopping potential (in *V*), E_{pseudo}^{i} is the standard redox potential of the pseudocapacitive current (in V), E_{pseudo}^{f} is the final potential of the pseudocapacitive current (in *V*), and φ_{pseudo}^{i} is the neighboring pseudocapacitive current (dimensionless current). For the first time, herein we thus propose a homogeneous and universal formalism for simulating a voltammogram, irrespective of the origin of its redox dynamics, for all electrochemical energy storage materials, be they electrochemical double layer, purely battery-type or pseudocapacitive in nature. Moreover, via this formalism, we can show that all electrode materials possess a combination of these three contributions. However, the contribution of each of the components will then be more or less intense, depending on the value of the maximum current (i_{EDLC}^{max}, i_{pseudo}^{max}, i_{batt}^{max}), *i.e.*:

$$i_{tot} = i_{EDLC}^{max}\cdot\varphi_{EDLC} + i_{pseudo}^{max}\cdot\varphi_{pseudo} + i_{batt}^{max}\cdot\varphi_{batt} \quad \text{Eq.10.}$$

Fig. S11 shows CV profiles of various electrochemical systems, including $i_{peak} + i_{EDLC}$, pure i_{pseudo}, $i_{pseudo} + i_{EDLC}$**,** and the contour plots of % pseudo of these systems related to the resistance and scan rate. These results were obtained by using the Wolfram Language with its Mathematica tool to plot the functions according to the equation **Eq. 10**, where $A_{batt} = A_{EDLC} = A_{pseudo} = 1$ was considered. Firstly, the different current profiles of the first two models in **Fig. S11a** and **b**, with different values for R_s and ν, can be observed. These characteristics relate to different *%pseudo* as indicated in the contour plot (**Fig. S11c**). One can clearly see that, even when increasing the scan rate, the %pseudo still barely reaches 90% as a

result of the peak current contribution. This result agrees with experimental observations (see the ESI). Secondly, the rectangular CV profile (**Fig. S11d** and **e**) is distorted by the presence of i_{EDLC} current with a large $R_s = 50\Omega$. Similarly, **Fig. S11f** demonstrates %pseudo as a function of the R_s and the scan rate for a pseudocapacitive current with the contribution of i_{EDLC}. It was found that the *%pseudo* is high, even when increasing the scan rate. This result also agrees with experimental observations (Fig. S13-S60).

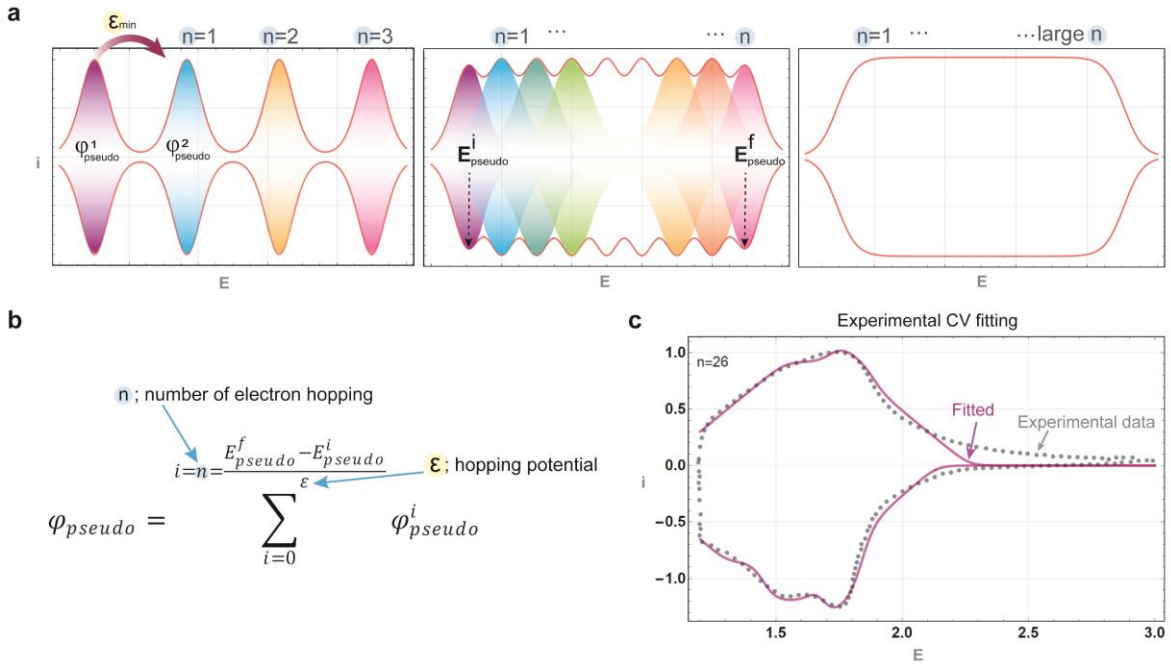

Fig. 4│ Formalism of the novel pseudocapacitor CV fitting method. (a) Pseudocapacitor CV of various numbers of electron hopping (or the number of redox centers, n) and the potential distribution (or hopping potential, ε). (b) The equation of pseudocapacitor signal. (c) Experimental CV fitted by our formalism.

Fig. 4a shows the proposed pseudocapacitor model where the redox peaks start to overlap with the number of electron hopping. The extended formalism from **Eq. 8** (as demonstrated in **Fig. 4b**) was finally introduced into the total current with other current components (Eq. 10). Using this model, an experimental CV was well fitted, as shown in **Fig. 4c**. It was also found that,

even in the battery materials, there is a certain pseudocapacitive contribution resulting from the distribution of the potential to the nearby redox centers when the number of redox centers per nm^3 is high, as presented in the corresponding matrix models with numerous redox centers (Fig. S13-S60).

The conventional method is to use the peak current to determine whether a device is a battery or a pseudocapacitor. While the peak current model is a good fit, the signal including all potential ranges is incomplete. Moreover, the model proposed herein has shown a strong correlation between state-of-the-art experience and reliable theory. Besides, this proposed theory is based on equilibrium exchange between two redox centers, so it cannot be used to analyse the reversibility of the charge-discharge process.

Conclusion

Batteries and supercapacitors are both widely used electrochemical energy storage technologies. When it comes to batteries, redox processes display unusual electrochemical behavior, for which there is no clear explanation to date. Complicating matters further, no universal analytical formalism for assessing voltammograms has thus far been proposed. This article began by discussing the electrochemical properties of batteries and pseudocapacitive materials, as well as what sets them apart while focusing on electron transport pathways. We have shown that battery and pseudocapacitor materials, called Faradaic electrode materials, both exhibit strong electron delocalization resulting in large redox potential distributions due to tunneling and the polaron effect. Perhaps more significantly, battery materials display the same potential dispersion, albeit weaker. Faradaic electrode materials are very much in the scientific limelight of late, and our research serves to provide a link between them all, thereby culminating in a ground-breaking, all-inclusive model for assessing such materials.

458

Reference

1. Simon, P.; Gogotsi, Y., Perspectives for electrochemical capacitors and related devices. *Nat Mater* **2020,** *19* (11), 1151-1163.

2. Ando, Y.; Okubo, M.; Yamada, A.; Otani, M., Capacitive versus Pseudocapacitive Storage in MXene. *Advanced Functional Materials* **2020,** *30* (47).

3. Augustyn, V.; Simon, P.; Dunn, B., Pseudocapacitive oxide materials for high-rate electrochemical energy storage. *Energy & Environmental Science* **2014,** *7* (5).

4. Come, J.; Augustyn, V.; Kim, J. W.; Rozier, P.; Taberna, P.-L.; Gogotsi, P.; Long, J. W.; Dunn, B.; Simon, P., Electrochemical Kinetics of Nanostructured Nb2O5Electrodes. *Journal of The Electrochemical Society* **2014,** *161* (5), A718-A725.

5. Come, J.; Taberna, P. L.; Hamelet, S.; Masquelier, C.; Simon, P., Electrochemical Kinetic Study of LiFePO4 Using Cavity Microelectrode. *Journal of The Electrochemical Society* **2011,** *158* (10).

6. Costentin, C.; Porter, T. R.; Saveant, J. M., How Do Pseudocapacitors Store Energy? Theoretical Analysis and Experimental Illustration. *ACS Appl Mater Interfaces* **2017,** *9* (10), 8649-8658.

7. Choi, C.; Ashby, D. S.; Butts, D. M.; DeBlock, R. H.; Wei, Q.; Lau, J.; Dunn, B., Achieving high energy density and high power density with pseudocapacitive materials. *Nature Reviews Materials* **2019,** *5* (1), 5-19.

8. Brousse, T.; Bélanger, D.; Long, J. W., To Be or Not To Be Pseudocapacitive? *Journal of The Electrochemical Society* **2015,** *162* (5), A5185-A5189.

9. M. Toupin, T. Brousse., D. Bélanger, Charge storage mechanism of MnO2 electrode used in aqueous electrochemical capacitor. *Chem. Mater.* **2004,** *16*, 3184–3190.

10. Liu, T.; Finn, L.; Yu, M.; Wang, H.; Zhai, T.; Lu, X.; Tong, Y.; Li, Y., Polyaniline and polypyrrole pseudocapacitor electrodes with excellent cycling stability. *Nano Lett* **2014,** *14* (5), 2522-7.

11. A.Aegerter, M., Sol–gel niobium pentoxide: A promising material for electrochromic coatings, batteries, nanocrystalline solar cells and catalysis. *Solar Energy Materials and Solar Cells* **2001,** *68* (3-4), 401-422.

12. Arias, C. R.; Debiemme-Chouvy, C.; Gabrielli, C.; Laberty-Robert, C.; Pailleret, A.; Perrot, H.; Sel, O., New Insights into Pseudocapacitive Charge-Storage Mechanisms in Li-Birnessite Type MnO2 Monitored by Fast Quartz Crystal Microbalance Methods. *The Journal of Physical Chemistry C* **2014,** *118* (46), 26551-26559.

13. Chen, D.; Ding, D.; Li, X.; Waller, G. H.; Xiong, X.; El-Sayed, M. A.; Liu, M., Probing the Charge Storage Mechanism of a Pseudocapacitive MnO2 Electrode Using in Operando Raman Spectroscopy. *Chemistry of Materials* **2015,** *27* (19), 6608-6619.

14. Chigane, M. I., M. , Manganese Oxide Thin Film Preparation by Potentiostatic Electrolyses and Electrochromism. *J. Electrochem. Soc.* **2000,** *147*, 2246

15. Cong, S.; Tian, Y.; Li, Q.; Zhao, Z.; Geng, F., Single-crystalline tungsten oxide quantum dots for fast pseudocapacitor and electrochromic applications. *Adv Mater* **2014,** *26* (25), 4260-7.

16. Ganeshan, K.; Shin, Y. K.; Osti, N. C.; Sun, Y.; Prenger, K.; Naguib, M.; Tyagi, M.; Mamontov, E.; Jiang, D. E.; van Duin, A. C. T., Structure and Dynamics of Aqueous Electrolytes Confined in 2D-TiO2/Ti3C2T2 MXene Heterostructures. *ACS Appl Mater Interfaces* **2020,** *12* (52), 58378-58389.

17. Jabeen, N.; Xia, Q.; Savilov, S. V.; Aldoshin, S. M.; Yu, Y.; Xia, H., Enhanced Pseudocapacitive Performance of alpha-MnO2 by Cation Preinsertion. *ACS Appl Mater Interfaces* **2016,** *8* (49), 33732-33740.

18. Jadon, A.; Prabhudev, S.; Buvat, G.; Patnaik, S. G.; Djafari-Rouhani, M.; Estève, A.; Guay, D.; Pech, D., Rethinking Pseudocapacitance: A Way to Harness Charge Storage of Crystalline RuO2. *ACS Applied Energy Materials* **2020,** *3* (5), 4144-4148.

19. Ji, X.; Xu, K.; Chen, C.; Zhang, B.; Ruan, Y.; Liu, J.; Miao, L.; Jiang, J., Probing the electrochemical capacitance of MXene nanosheets for high-performance pseudocapacitors. *Phys Chem Chem Phys* **2016,** *18* (6), 4460-7.

20. Juodkazis, K.; Juodkazytė, J.; Šukienė, V.; Grigucevičienė, A.; Selskis, A., On the charge storage mechanism at RuO2/0.5 M H2SO4 interface. *Journal of Solid State Electrochemistry* **2007,** *12* (11), 1399-1404.

21. Lee, C. Y.; Bond, A. M., Revelation of multiple underlying RuO2 redox processes associated with pseudocapacitance and electrocatalysis. *Langmuir* **2010,** *26* (20), 16155-62.

22. Lee, M.-T.; Tsai, W.-T.; Deng, M.-J.; Cheng, H.-F.; Sun, I. W.; Chang, J.-K., Pseudocapacitance of MnO2 originates from reversible insertion/desertion of thiocyanate anions studied using in situ X-ray absorption spectroscopy in ionic liquid electrolyte. *Journal of Power Sources* **2010,** *195* (3), 919-922.

23. Leong, Z. Y.; Yang, H. Y., A Study of MnO2 with Different Crystalline Forms for Pseudocapacitive Desalination. *ACS Appl Mater Interfaces* **2019,** *11* (14), 13176-13184.

24. Liu, Y.; Zhou, F.; Ozolins, V., Ab Initio Study of the Charge-Storage Mechanisms in RuO2-Based Electrochemical Ultracapacitors. *The Journal of Physical Chemistry C* **2011,** *116* (1), 1450-1457.

25. Llordes, A.; Garcia, G.; Gazquez, J.; Milliron, D. J., Tunable near-infrared and visible-light transmittance in nanocrystal-in-glass composites. *Nature* **2013,** *500* (7462), 323-6.

26. Lukatskaya, M. R.; Bak, S.-M.; Yu, X.; Yang, X.-Q.; Barsoum, M. W.; Gogotsi, Y., Probing the Mechanism of High Capacitance in 2D Titanium Carbide Using In Situ X-Ray Absorption Spectroscopy. *Advanced Energy Materials* **2015,** *5* (15).

27. Sakai, N., Ebina, Y., Takada, K. & Sasaki, T. , Electrochromic Films Composed of MnO2 Nanosheets with Controlled Optical Density and High Coloration Efficiency. *J. Electrochem. Soc.* **2005,** *152*.

28. Scherer, M. R.; Li, L.; Cunha, P. M.; Scherman, O. A.; Steiner, U., Enhanced electrochromism in gyroid-structured vanadium pentoxide. *Adv Mater* **2012,** *24* (9), 1217-21.

29. Shao, H.; Xu, K.; Wu, Y.-C.; Iadecola, A.; Liu, L.; Ma, H.; Qu, L.; Raymundo-Piñero, E.; Zhu, J.; Lin, Z.; Taberna, P.-L.; Simon, P., Unraveling the Charge Storage Mechanism of Ti3C2Tx MXene Electrode in Acidic Electrolyte. *ACS Energy Letters* **2020,** *5* (9), 2873-2880.

30. Sopčić, S.; Roković, M. K.; Mandić, Z.; Róka, A.; Inzelt, G., Mass changes accompanying the pseudocapacitance of hydrous RuO2 under different experimental conditions. *Electrochimica Acta* **2011,** *56* (10), 3543-3548.

31. Sun, P.; Deng, Z.; Yang, P.; Yu, X.; Chen, Y.; Liang, Z.; Meng, H.; Xie, W.; Tan, S.; Mai, W., Freestanding CNT–WO3 hybrid electrodes for flexible asymmetric supercapacitors. *Journal of Materials Chemistry A* **2015,** *3* (22), 12076-12080.

32. Tian, Y.; Cong, S.; Su, W.; Chen, H.; Li, Q.; Geng, F.; Zhao, Z., Synergy of W18O49 and polyaniline for smart supercapacitor electrode integrated with energy level indicating functionality. *Nano Lett* **2014,** *14* (4), 2150-6.

33. Watanabe, E.; Ushiyama, H.; Yamashita, K.; Morikawa, Y.; Asakura, D.; Okubo, M.; Yamada, A., Charge Storage Mechanism of RuO2/Water Interfaces. *The Journal of Physical Chemistry C* **2017,** *121* (35), 18975-18981.

34. Wei, D.; Scherer, M. R.; Bower, C.; Andrew, P.; Ryhanen, T.; Steiner, U., A nanostructured electrochromic supercapacitor. *Nano Lett* **2012,** *12* (4), 1857-62.

35. Wei, Q.; Liu, J.; Feng, W.; Sheng, J.; Tian, X.; He, L.; An, Q.; Mai, L., Hydrated vanadium pentoxide with superior sodium storage capacity. *Journal of Materials Chemistry A* **2015,** *3* (15), 8070-8075.

36. Wojtek Dmowski, T. E., Karen E. Swider-Lyons, Corey T. Love, and Debra R. Rolison, Local Atomic Structure and Conduction Mechanism of Nanocrystalline Hydrous RuO2 from X-ray Scattering. *J. Phys. Chem. B*.

37. Xie, Z.; Jin, X.; Chen, G.; Xu, J.; Chen, D.; Shen, G., Integrated smart electrochromic windows for energy saving and storage applications. *Chem Commun (Camb)* **2014,** *50* (5), 608-10.

38. Yang, P.; Sun, P.; Chai, Z.; Huang, L.; Cai, X.; Tan, S.; Song, J.; Mai, W., Large-scale fabrication of pseudocapacitive glass windows that combine electrochromism and energy storage. *Angew Chem Int Ed Engl* **2014,** *53* (44), 11935-9.

39. Yang, P.; Sun, P.; Du, L.; Liang, Z.; Xie, W.; Cai, X.; Huang, L.; Tan, S.; Mai, W., Quantitative Analysis of Charge Storage Process of Tungsten Oxide that Combines Pseudocapacitive and Electrochromic Properties. *The Journal of Physical Chemistry C* **2015,** *119* (29), 16483-16489.

40. Yang, P.; Sun, P.; Mai, W., Electrochromic energy storage devices. *Materials Today* **2016,** *19* (7), 394-402.

41. Yoshida, N.; Yamada, Y.; Nishimura, S.-i.; Oba, Y.; Ohnuma, M.; Yamada, A., Unveiling the Origin of Unusual Pseudocapacitance of RuO2·nH2O from Its Hierarchical Nanostructure by Small-Angle X-ray Scattering. *The Journal of Physical Chemistry C* **2013,** *117* (23), 12003-12009.

42. Zhan, C.; Jiang, D. E., Understanding the pseudocapacitance of RuO2 from joint density functional theory. *J Phys Condens Matter* **2016,** *28* (46), 464004.

43. Zhan, C.; Naguib, M.; Lukatskaya, M.; Kent, P. R. C.; Gogotsi, Y.; Jiang, D. E., Understanding the MXene Pseudocapacitance. *J Phys Chem Lett* **2018,** *9* (6), 1223-1228.

44. Zhu, Y.-P.; Xia, C.; Lei, Y.; Singh, N.; Schwingenschlögl, U.; Alshareef, H. N., Solubility contrast strategy for enhancing intercalation pseudocapacitance in layered MnO2 electrodes. *Nano Energy* **2019,** *56*, 357-364.

45. Bhagwan, J.; Kumar, N.; Yadav, K. L.; Sharma, Y., Probing the electrical properties and energy storage performance of electrospun ZnMn2O4 nanofibers. *Solid State Ionics* **2018,** *321*, 75-82.

586 46. Blidberg, A.; Gustafsson, T.; Tengstedt, C.; Björefors, F.; Brant, W. R., Monitoring
587 LixFeSO4F (x = 1, 0.5, 0) Phase Distributions in Operando To Determine Reaction
588 Homogeneity in Porous Battery Electrodes. *Chemistry of Materials* **2017,** *29* (17), 7159-7169.

589 47. Chen, Z.; Xu, F.; Cao, S.; Li, Z.; Yang, H.; Ai, X.; Cao, Y., High Rate, Long Lifespan
590 LiV3 O8 Nanorods as a Cathode Material for Lithium-Ion Batteries. *Small* **2017,** *13* (18).

591 48. Dong, R.; Ye, Q.; Kuang, L.; Lu, X.; Zhang, Y.; Zhang, X.; Tan, G.; Wen, Y.; Wang,
592 F., Enhanced supercapacitor performance of Mn3O4 nanocrystals by doping transition-metal
593 ions. *ACS Appl Mater Interfaces* **2013,** *5* (19), 9508-16.

594 49. Drozhzhin, O. A.; Tertov, I. V.; Alekseeva, A. M.; Aksyonov, D. A.; Stevenson, K. J.;
595 Abakumov, A. M.; Antipov, E. V., β-NaVP2O7 as a Superior Electrode Material for Na-Ion
596 Batteries. *Chemistry of Materials* **2019,** *31* (18), 7463-7469.

597 50. Du, J.; Jiao, L.; Wu, Q.; Liu, Y.; Zhao, Y.; Guo, L.; Wang, Y.; Yuan, H., Synthesis and
598 characterization of Li2FeP2O7/C nanocomposites as cathode materials for Li-ion batteries.
599 *Electrochimica Acta* **2013,** *103*, 219-225.

600 51. Geng, X.; Zhang, Y.; Han, Y.; Li, J.; Yang, L.; Benamara, M.; Chen, L.; Zhu, H., Two-
601 Dimensional Water-Coupled Metallic MoS2 with Nanochannels for Ultrafast Supercapacitors.
602 *Nano Lett* **2017,** *17* (3), 1825-1832.

603 52. Goikolea, E.; Daffos, B.; Taberna, P. L.; Simon, P., Synthesis of nanosized MnO2
604 prepared by the polyol method and its application in high power supercapacitors. *Materials for*
605 *Renewable and Sustainable Energy* **2013,** *2* (3-4).

606 53. Guo, D.; Zhang, H.; Yu, X.; Zhang, M.; Zhang, P.; Li, Q.; Wang, T., Facile synthesis
607 and excellent electrochemical properties of CoMoO4 nanoplate arrays as supercapacitors.
608 *Journal of Materials Chemistry A* **2013,** *1* (24).

609 54. He, D.; Wu, T.; Wang, B.; Yang, Y.; Zhao, S.; Wang, J.; Yu, H., Novel Na2TiSiO5
610 anode material for lithium ion batteries. *Chem Commun (Camb)* **2019,** *55* (15), 2234-2237.

611 55. Inamdar, A. I.; Ahmed, A. T. A.; Chavan, H. S.; Jo, Y.; Cho, S.; Kim, J.; Pawar, S. M.;
612 Hou, B.; Cha, S.; Kim, H.; Im, H., Influence of operating temperature on Li2ZnTi3O8 anode
613 performance and high-rate charging activity of Li-ion battery. *Ceramics International* **2018,**
614 *44* (15), 18625-18632.

615 56. Jang, H.; Jin, W.; Nam, G.; Yoo, Y.; Jeon, J. S.; Park, J.; Kim, M. G.; Cho, J., Exploring
616 the artificially induced nonstoichiometric effect of Li2RuO3 as a reactive promoter on
617 electrocatalytic behavior. *Energy & Environmental Science* **2020,** *13* (7), 2167-2177.

618 57. Jenkins, T.; Alarco, J. A.; Mackinnon, I. D. R., Synthesis and Characterization of a
619 Novel Hydrated Layered Vanadium(III) Phosphate Phase K3V3(PO4)4.H2O: A Functional
620 Cathode Material for Potassium-Ion Batteries. *ACS Omega* **2021,** *6* (3), 1917-1929.

621 58. Kim, J. W.; Augustyn, V.; Dunn, B., The Effect of Crystallinity on the Rapid
622 Pseudocapacitive Response of Nb2O5. *Advanced Energy Materials* **2012,** *2* (1), 141-148.

623 59. Kwon, N. H.; Yin, H.; Vavrova, T.; Lim, J. H. W.; Steiner, U.; Grobéty, B.; Fromm, K.
624 M., Nanoparticle shapes of LiMnPO4, Li+ diffusion orientation and diffusion coefficients for
625 high volumetric energy Li+ ion cathodes. *Journal of Power Sources* **2017,** *342*, 231-240.

626 60. Lu, J.; Ran, H.; Li, J.; Wan, J.; Wang, C.; Ji, P.; Wang, X.; Liu, G.; Hu, C., A fast
627 composite-hydroxide-mediated approach for synthesis of 2D-LiCoO2 for high performance
628 asymmetric supercapacitor. *Electrochimica Acta* **2020,** *331*.

61. Lu, X.; Yu, M.; Zhai, T.; Wang, G.; Xie, S.; Liu, T.; Liang, C.; Tong, Y.; Li, Y., High energy density asymmetric quasi-solid-state supercapacitor based on porous vanadium nitride nanowire anode. *Nano Lett* **2013,** *13* (6), 2628-33.

62. Lukatskaya, M. R. e. a., Cation Intercalation and High Volumetric Capacitance of Two-Dimensional Titanium Carbide. *Science* **2013,** *341*, 1502–1505.

63. Malaie, K.; Scholz, F., Realizing alkaline all-pseudocapacitive supercapacitors based on highly stable nanospinel oxide coatings. *Colloids and Surfaces A: Physicochemical and Engineering Aspects* **2019,** *577*, 576-582.

64. Mu, J.; Wang, J.; Hao, J.; Cao, P.; Zhao, S.; Zeng, W.; Miao, B.; Xu, S., Hydrothermal synthesis and electrochemical properties of V2O5 nanomaterials with different dimensions. *Ceramics International* **2015,** *41* (10), 12626-12632.

65. Nithya, V. D.; Pandi, K.; Lee, Y. S.; Selvan, R. K., Synthesis, characterization and electrochemical performances of nanocrystalline FeVO4 as negative and LiCoPO4 as positive electrode for asymmetric supercapacitor. *Electrochimica Acta* **2015,** *167*, 97-104.

66. Opitz, M.; Yue, J.; Wallauer, J.; Smarsly, B.; Roling, B., Mechanisms of Charge Storage in Nanoparticulate TiO2 and Li4Ti5O12 Anodes: New Insights from Scan rate-dependent Cyclic Voltammetry. *Electrochimica Acta* **2015,** *168*, 125-132.

67. Qu, L.; Liu, Y.; Fang, S.; Yang, L.; Hirano, S.-i., Li 2 FeSiO 4 coated by sorbitanlaurat-derived carbon as cathode of high-performance lithium-ion battery. *Electrochimica Acta* **2015,** *163*, 123-131.

68. Rakhi, R. B.; Ahmed, B.; Hedhili, M. N.; Anjum, D. H.; Alshareef, H. N., Effect of Postetch Annealing Gas Composition on the Structural and Electrochemical Properties of Ti2CTx MXene Electrodes for Supercapacitor Applications. *Chemistry of Materials* **2015,** *27* (15), 5314-5323.

69. Rakhi, R. B.; Chen, W.; Cha, D.; Alshareef, H. N., Substrate dependent self-organization of mesoporous cobalt oxide nanowires with remarkable pseudocapacitance. *Nano Lett* **2012,** *12* (5), 2559-67.

70. Sahoo, S.; Ratha, S.; Rout, C. S., Spinel NiCo₂O₄ Nanorods for Supercapacitor Applications. *American Journal of Engineering and Applied Sciences* **2015,** *8* (3), 371-379.

71. Shafi, P. M.; Joseph, N.; Thirumurugan, A.; Bose, A. C., Enhanced electrochemical performances of agglomeration-free LaMnO3 perovskite nanoparticles and achieving high energy and power densities with symmetric supercapacitor design. *Chemical Engineering Journal* **2018,** *338*, 147-156.

72. Shan, Q.; Mu, X.; Alhabeb, M.; Shuck, C. E.; Pang, D.; Zhao, X.; Chu, X.-F.; Wei, Y.; Du, F.; Chen, G.; Gogotsi, Y.; Gao, Y.; Dall'Agnese, Y., Two-dimensional vanadium carbide (V2C) MXene as electrode for supercapacitors with aqueous electrolytes. *Electrochemistry Communications* **2018,** *96*, 103-107.

73. Shen, L.; Chen, S.; Maier, J.; Yu, Y., Carbon-Coated Li3 VO4 Spheres as Constituents of an Advanced Anode Material for High-Rate Long-Life Lithium-Ion Batteries. *Adv Mater* **2017,** *29* (33).

74. Singh, P.; Shiva, K.; Celio, H.; Goodenough, J. B., Eldfellite, NaFe(SO4)2: an intercalation cathode host for low-cost Na-ion batteries. *Energy & Environmental Science* **2015,** *8* (10), 3000-3005.

673 75. Vattikuti, S. V. P.; Devarayapalli, K. C.; Dang, N. N.; Shim, J., 1D/1D
674 Na2Ti3O7/SWCNTs electrode for split-cell-type asymmetric supercapacitor device. *Ceramics*
675 *International* **2021,** *47* (8), 11602-11610.

676 76. Vignesh, V.; Subramani, K.; Sathish, M.; Navamathavan, R., Electrochemical
677 investigation of manganese ferrites prepared via a facile synthesis route for supercapacitor
678 applications. *Colloids and Surfaces A: Physicochemical and Engineering Aspects* **2018,** *538*,
679 668-677.

680 77. Vincent, R. C.; Vishnoi, P.; Preefer, M. B.; Shen, J. X.; Seeler, F.; Persson, K. A.;
681 Seshadri, R., Li5VF4(SO4)2: A Prototype High-Voltage Li-Ion Cathode. *ACS Appl Mater*
682 *Interfaces* **2020,** *12* (43), 48662-48668.

683 78. Vujković, M.; Mitrić, M.; Mentus, S., High-rate intercalation capability of NaTi 2 (PO
684 4) 3 /C composite in aqueous lithium and sodium nitrate solutions. *Journal of Power Sources*
685 **2015,** *288*, 176-186.

686 79. Wang, D.; Xiao, J.; Xu, W.; Nie, Z.; Wang, C.; Graff, G.; Zhang, J.-G., Preparation and
687 electrochemical investigation of Li2CoPO4F cathode material for lithium-ion batteries.
688 *Journal of Power Sources* **2011,** *196* (4), 2241-2245.

689 80. Whiteley, Justin M.; Hafner, S.; Han, S. S.; Kim, S. C.; Le, V.-D.; Ban, C.; Kim, Y. H.;
690 Oh, K. H.; Lee, S.-H., All-solid-state disordered LiTiS2pseudocapacitor. *Journal of Materials*
691 *Chemistry A* **2017,** *5* (30), 15661-15668.

692 81. Wu, C.; Wu, Z. G.; Zhang, X.; Rajagopalan, R.; Zhong, B.; Xiang, W.; Chen, M.; Li,
693 H.; Chen, T.; Wang, E.; Yang, Z.; Guo, X., Insight into the Origin of Capacity Fluctuation of
694 Na2Ti6O13 Anode in Sodium Ion Batteries. *ACS Appl Mater Interfaces* **2017,** *9* (50), 43596-
695 43602.

696 82. Xiao, J.; Wen, J.; Zhao, J.; Ma, X.; Gao, H.; Zhang, X., A safe etching route to
697 synthesize highly crystalline Nb2CTx MXene for high performance asymmetric supercapacitor
698 applications. *Electrochimica Acta* **2020,** *337*.

699 83. Xiao, P. F.; Lai, M. O.; Lu, L., Transport and electrochemical properties of high
700 potential tavorite LiVPO4F. *Solid State Ionics* **2013,** *242*, 10-19.

701 84. Xu, H.; Shu, J.; Hu, X.; Sun, Y.; Luo, W.; Huang, Y., Electrospun porous LiNb3O8
702 nanofibers with enhanced lithium-storage properties. *Journal of Materials Chemistry A* **2013,**
703 *1* (47).

704 85. Xu, W.; Jiang, Z.; Yang, Q.; Huo, W.; Javed, M. S.; Li, Y.; Huang, L.; Gu, X.; Hu, C.,
705 Approaching the lithium-manganese oxides' energy storage limit with Li2MnO3 nanorods for
706 high-performance supercapacitor. *Nano Energy* **2018,** *43*, 168-176.

707 86. Yang, Y. e. a., Hydrothermally Formed Three-Dimensional Nanoporous Ni(OH) 2
708 Thin-Film Supercapacitors. *Nano Lett.* **2014,** *12*, 2559–2567.

709 87. Zhang, J. e. a., Template Synthesis of Tubular Ruthenium Oxides for Supercapacitor
710 Applications. *J. Phys. Chem. C* **2010,** *114*, 13608–13613.

711 88. Zhang, Y.; Ding, Z.; Foster, C. W.; Banks, C. E.; Qiu, X.; Ji, X., Oxygen Vacancies
712 Evoked Blue TiO2(B) Nanobelts with Efficiency Enhancement in Sodium Storage Behaviors.
713 *Advanced Functional Materials* **2017,** *27* (27).

714 89. Zhao, G.; Zhang, N.; Sun, K., Porous MoO3 films with ultra-short relaxation time used
715 for supercapacitors. *Materials Research Bulletin* **2013,** *48* (3), 1328-1332.

90. Zheng, J.-c.; Han, Y.-d.; Tang, L.-b.; Zhang, B., Investigation of phase structure change and electrochemical performance in LiVP2O7-Li3V2(PO4)3-LiVPO4F system. *Electrochimica Acta* **2016,** *198*, 195-202.

91. Zhu, H.; He, H.; Xin, X.; Ma, X.; Zan, L.; Zhang, Y., Facile synthesis of Li2MnSiO4/C/graphene composite with superior high-rate performances as cathode materials for Li-ion batteries. *Electrochimica Acta* **2015,** *155*, 116-124.

92. J.W. Long, K. E. S., C.I. Merzbacher, D.R. Rolison, Voltammetric Characterization of Ruthenium Oxide-Based Aerogels and Other RuO2 Solids: The Nature of Capacitance in Nanostructured Materials. *Langmuir* **1999,** *15*, 780–784.

93. Sugimoto, W.; Yokoshima, K.; Murakami, Y.; Takasu, Y., Charge storage mechanism of nanostructured anhydrous and hydrous ruthenium-based oxides. *Electrochimica Acta* **2006,** *52* (4), 1742-1748.

94. Liu, J.; Wang, J.; Ni, Y.; Zhang, K.; Cheng, F.; Chen, J., Recent breakthroughs and perspectives of high-energy layered oxide cathode materials for lithium ion batteries. *Materials Today* **2021,** *43*, 132-165.

95. Kim, H.-J.; Krishna, T. N. V.; Zeb, K.; Rajangam, V.; Gopi, C. V. V. M.; Sambasivam, S.; Raghavendra, K. V. G.; Obaidat, I. M., A Comprehensive Review of Li-Ion Battery Materials and Their Recycling Techniques. *Electronics* **2020,** *9* (7).

96. Trasatti, S. B., G., A new interesting electrode material. Solid state structure and electrochemical behaviour. *J. Electroanal. Chem.* **1971,** *29*, 4-8.

97. Marcus, R. A., On the Theory of Electron-Transfer Reactions. VI. Unified Treatment for Homogeneous and Electrode Reactions. *The Journal of Chemical Physics* **1965,** *43* (2), 679-701.

98. <J. M. Savéant, J. Phys. Chem. B, 106 (2002) 9387.pdf>.

99. Fraggedakis, D.; McEldrew, M.; Smith, R. B.; Krishnan, Y.; Zhang, Y.; Bai, P.; Chueh, W. C.; Shao-Horn, Y.; Bazant, M. Z., Theory of coupled ion-electron transfer kinetics. *Electrochimica Acta* **2021,** *367*.

100. Franchini, C.; Reticcioli, M.; Setvin, M.; Diebold, U., Polarons in materials. *Nature Reviews Materials* **2021,** *6* (7), 560-586.

101. Costentin, C., Electrochemical Energy Storage: Questioning the Popular v/v(1/2) Scan Rate Diagnosis in Cyclic Voltammetry. *J Phys Chem Lett* **2020,** *11* (22), 9846-9849.

102. Forghani, M.; Donne, S. W., Method Comparison for Deconvoluting Capacitive and Pseudo-Capacitive Contributions to Electrochemical Capacitor Electrode Behavior. *Journal of The Electrochemical Society* **2018,** *165* (3), A664-A673.

103. Chen, G. Z., Linear and non-linear pseudocapacitances with or without diffusion control. *Progress in Natural Science: Materials International* **2021,** *31* (6), 792-800.

104. Yu, L. P.; Chen, G. Z., Redox electrode materials for supercapatteries. *Journal of Power Sources* **2016,** *326* (15), 604-612.

105. Oh, S. W., Bang, H. J., Bae, Y. C., Sun, Y.-K.; Effect of calcination temperature on morphology, crystallinity and electrochemical properties of nano-crystalline metal oxides (Co3O4, CuO, and NiO) prepared via ultrasonic spray pyrolysis. *Journal of Power Sources* **2007,** *173* (1), 502-509.

106. Anasori, B., Lukatskaya, M. R., Gogotsi, Y.; 2D metal carbides and nitrides (MXenes) for energy storage. *Nature Reviews Materials* **2017,** *2* (2), 16098.

107. Hu, M.; Zhang, H.; Hu, T.; Fan, B.; Wang, X.; Li, Z. Emerging 2D MXenes for supercapacitors: status, challenges and prospects. *Chemical Society Reviews* **2020,** *49* (18), 6666-6693.

108. Augustyn, V.; Simon, P.; Dunn, B. Pseudocapacitive oxide materials for high-rate electrochemical energy storage. *Energy & Environmental Science* **2014**, *7* (5), 1597-1614.

109. Jiang, Y.; Liu, J. Definitions of Pseudocapacitive Materials: A Brief Review. *ENERGY & ENVIRONMENTAL MATERIALS* **2019**, *2* (1), 30-37.

110. Choi, C.; Ashby, D. S.; Butts, D. M.; DeBlock, R. H.; Wei, Q.; Lau, J.; Dunn, B. Achieving high energy density and high power density with pseudocapacitive materials. *Nature Reviews Materials* **2020**, *5* (1), 5-19.

111. Li, X.; Huang, Z.; Shuck, C. E.; Liang, G.; Gogotsi, Y.; Zhi, C. MXene chemistry, electrochemistry and energy storage applications. *Nature Reviews Chemistry* **2022**, *6* (6), 389-404.

112. Dupont, M. F.; Donne, S. W. Charge storage mechanisms in electrochemical capacitors: Effects of electrode properties on performance. Journal of Power Sources 2016, 326, 613-623.

113. Forghani, M.; Donne, S. W. Method Comparison for Deconvoluting Capacitive and Pseudo-Capacitive Contributions to Electrochemical Capacitor Electrode Behavior. Journal of The Electrochemical Society 2018, 165 (3), A664-A673.

114. Fleischmann, S.; Zhang, Y.; Wang, X.; Cummings, P. T.; Wu, J.; Simon, P.; Gogotsi, Y.; Presser, V.; Augustyn, V. Continuous transition from double-layer to Faradaic charge storage in confined electrolytes. Nature Energy 2022, 7 (3), 222-228.

115. Deebansok, S.; Deng, J.; Le Calvez, E.; Zhu, Y.; Crosnier, O.; Brousse, T.; Fontaine, O. Capacitive tendency concept alongside supervised machine-learning toward classifying electrochemical behavior of battery and pseudocapacitor materials. *Nature Communications* **2024**, *15* (1), 1133. DOI: 10.1038/s41467-024-45394-w.

116. Wang, J.; Polleux, J.; Lim, J.; Dunn, B. Pseudocapacitive Contributions to Electrochemical Energy Storage in TiO2 (Anatase) Nanoparticles. *The Journal of Physical Chemistry C* **2007**, *111* (40), 14925-14931. DOI: 10.1021/jp074464w.